Spectral multiplexing method for digital snapshot spectral imaging

Michael A. Golub,[1,*] Menachem Nathan,[1] Amir Averbuch,[2] Eitan Lavi,[2] Valery A. Zheludev,[2] and Alon Schclar[2]

[1]Department of Physical Electronics, Faculty of Engineering, Tel Aviv University, Ramat Aviv 69978, Israel

[2]School of Computer Science, Faculty of Exact Sciences, Tel Aviv University, Ramat Aviv 69978, Israel

*Corresponding author: mgolub@eng.tau.ac.il

Received 27 October 2008; revised 5 February 2009; accepted 6 February 2009; posted 13 February 2009 (Doc. ID 103259); published 4 March 2009

We propose a spectral imaging method for piecewise "macropixel" objects, which allows a regular digital camera to be converted into a digital snapshot spectral imager by equipping the camera with only a disperser and a demultiplexing algorithm. The method exploits a "multiplexed spectrum" intensity pattern, i.e., the superposition of spectra from adjacent different image points, formed on the image sensor of the digital camera. The spatial image resolution is restricted to a macropixel level in order to acquire both spectral and spatial data (i.e., an entire spectral cube) in a single snapshot. Results of laboratory experiments with a special macropixel object image, composed of small, spatially uniform squares, provide to our knowledge a first verification of the proposed spectral imaging method.

OCIS codes: 110.4234, 300.6190, 260.2030.

1. Introduction

Spectral imaging (SI) provides a two-dimensional (2D) image of a polychromatic object or scene, separately in several bands of the spectrum [1]. Mosaic spectral filter arrays on an image sensor [2] lead to unacceptable light gathering losses and involve technological difficulties. The most straightforward way to perform SI is to use a removable set of narrow bandpass filters [3] or dynamic spectral filters [4]. High quality SI systems exploit "staring" or "push-broom" imagers [5]. Neither provides a "snapshot" SI mode for fast changing objects with an unpredictable development along the time scale, where the entire spectral cube needs to be acquired simultaneously and instantaneously in one "shot." Snapshot spectral imagers are usually based either on non-scanning computed tomographic imaging spectrometer (CTIS) designs [6–12] or on coded aperture spectral imager designs [13,14] and require a field stop and additional intermediate image formation optics.

A wide class of SI applications naturally involves objects with a piecewise structure composed of a set of "macropixels," all of which have the same uniform or another repeatable local spatial intensity distribution, whose wavelength spectrum varies from macropixel to macropixel. Examples of macropixel objects include images of reticle and wafer inspection equipment in the semiconductor industry, digitally printed patterns in the printing industry, and microwell array plates [15] and biochip microarrays [16,17] in chemistry and biology.

In this paper we show that snapshot spectral imaging of a piecewise macropixel object may be achieved by an exchange between spatial and spectral resolution using a regular digital camera. For this purpose, the digital camera needs to be equipped with a disperser whose entire chromatic dispersion matches the spatial extent of a single macropixel. We show theoretically and experimentally that the entire spectral cube may be obtained by applying digital demultiplexing algorithms to the multiplexed

0003-6935/09/081520-07$15.00/0

spectrum intensity pattern acquired in a single snapshot. Results of laboratory experiments with a macropixel object composed of small spatially uniform squares provide a proof of concept for our proposed method.

2. Nondispersed Macropixel Image

The term "nondispersed image" formed by a regular incoherent imaging system (like a digital camera) is contrasted below with the term "dispersed image" acquired through an imaging system equipped with a chromatic disperser. A "nondispersed" image is described by an intensity function $I(\mathbf{x},\lambda)$ of 2D Cartesian image coordinates $\mathbf{x}=(x,y)$ and the wavelength coordinate λ in a spectral range extending from $\lambda=\lambda_{\min}$ to $\lambda=\lambda_{\max}$.

Figure 1 shows a spectral cube and its relation to the discrete pixelated structure of an image sensor, which may be characterized by a 2D spatial pitch $\delta_x \times \delta_y$ and a limited number of pixels $N_x \times N_y$. The necessity of accessing a required number S of discrete spectral (wavelength) bands naturally reduces the amount of spatial data $K_x \times K_y$ provided by the image sensor at every spectral band, by about a factor S. Therefore an area of a minimal spatial feature size of the nondispersed image has to be about S times larger than the area $\delta_x\delta_y$ of a single image sensor pixel. We introduce a rectangular macropixel containing $S_x \times S_y$ pixels with a size $\Delta_x \times \Delta_y$,

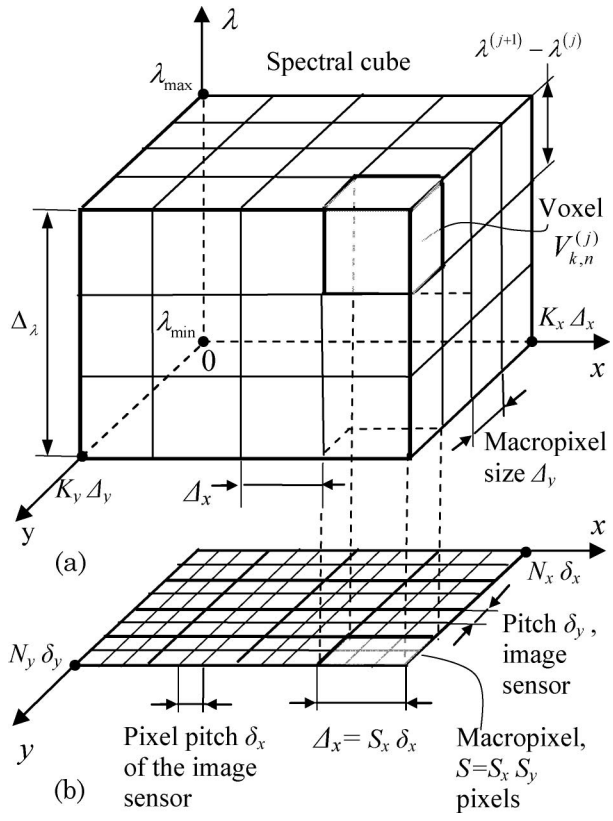

Fig. 1. Relation between (a) the spectral cube data and (b) the image on the sensor.

$$\Delta_x = S_x\delta_x, \qquad \Delta_y = S_y\delta_y, \qquad S_xS_y \geq S, \tag{1}$$

defining spatial dimensions of each voxel of the nondispersed image. Each voxel has a spectral dimension $\lambda^{(j+1)}-\lambda^{(j)}$, where $\lambda^{(j)}$ is a representative wavelength of the spectral band numbered $j=\overline{1,S}$. An entire wavelength range $\Delta_\lambda=\lambda_{\max}-\lambda_{\min}$ comprises a column of S voxels of the spectral cube, in accordance with the S wavelength bands. Equation (1) indicates that the S voxels in a column of the spectral cube correspond to $S_x \times S_y \geq S$ pixels at the image sensor, to keep a match between the total number of voxels acquired in the SI shot and the total number of image sensor pixels.

Each voxel is prescribed with a single value of the nondispersed image intensity $V_{k,n}^{(j)}$ at discrete raster points $\boldsymbol{\alpha}_{k,n}=(\alpha_{k,n},\beta_{k,n})$, where $k=\overline{1,K_y}$, $n=\overline{1,K_x}$, and $j=\overline{1,S}$. The nondispersed image of the macropixel object with local macropixel intensity distribution $g(\Delta\mathbf{x})\equiv g(\Delta x,\Delta y)$ is described by

$$I(\mathbf{x},\lambda^{(j)}) = \sum_{k=1}^{K_y}\sum_{n=1}^{K_x} V_{k,n}^{(j)} g(\mathbf{x}-\boldsymbol{\alpha}_{k,n}),$$
$$V_{k,n}^{(j)} = I(\boldsymbol{\alpha}_{k,n},\lambda^{(j)}). \tag{2}$$

3. Spectrum Multiplexing Model

Figure 2 shows the optical scheme of a SI imaging system that includes a camera lens L, an optional bandpass filter Φ for the spectral range from $\lambda_{\min}$ to $\lambda_{\max}$, a chromatic disperser G (prism or diffraction grating) positioned at the pupil, and an image sensor array D positioned at a focused image plane. The imaged object is a macropixel object composed of macropixels such as to form a macropixel image as described by Eq. (2).

In general, the direction $\mathbf{d}$ ($|\mathbf{d}|=1$) of the chromatic dispersion may not coincide with discrete raster directions. The disperser shifts laterally every single point image, relative to a nondispersed single point image position, by an amount $\zeta(\lambda)$ that is assumed to depend only on the wavelength λ within a field of view. An entire dispersive shift $\Delta\zeta=|\zeta(\lambda_{\max})-$

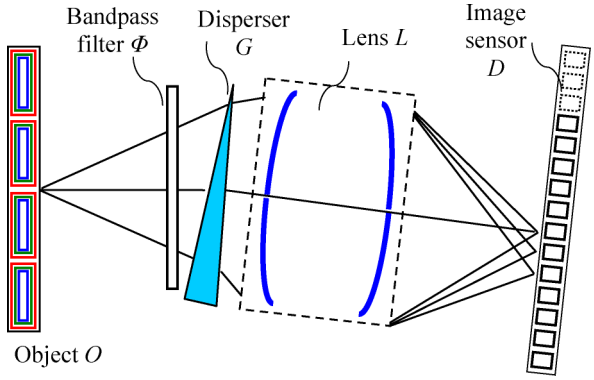

Fig. 2. (Color online) Optical arrangement of the experiment for spectral imaging with a prism disperser.

$\zeta(\lambda_{\min})|$ provides a straight-line "rainbow" of a dispersed point image.

The entire dispersed polychromatic image at the image sensor plane has a "multiplexed spectrum" intensity in the sense that data of different voxels are found at several adjacent spatial locations of the image plane. A "monochromatic mode" image sensor produces at a point $\mathbf{x}$ a signal proportional to the integral of the dispersed image intensity over all wavelengths

$$J(\mathbf{x}) = \int_{\lambda_{\mathrm{mun}}}^{\lambda_{\max}} \chi(\lambda) I[\mathbf{x} - \zeta(\lambda)\mathbf{d}, \lambda] \mathrm{d}\lambda$$

$$\cong \sum_{j=1}^{S} \chi^{(j)} I[\mathbf{x} - \zeta(\lambda^{(j)})\mathbf{d}, \lambda^{(j)}], \qquad (3)$$

where $\eta(\lambda)$ is a spectral response of the disperser, which in the case of a prism is just the transmittance coefficient and in the case of a diffraction grating is the diffraction efficiency of a performing diffraction order, $\kappa(\lambda)$ is the spectral sensitivity of the image sensor, $\chi(\lambda) = \kappa(\lambda)\eta(\lambda)$ is the combined spectral response of the dispersive element and the image sensor, and $\chi^{(j)} = \chi(\lambda^{(j)})[\lambda^{(j+1)} - \lambda^{(j)}]$ is a sampled version of $\chi(\lambda)\mathrm{d}\lambda$. Combining Eqs. (2) and (3) yields a multiplexed spectrum image of the macropixel object

$$J(\mathbf{x}) = \sum_{k=1}^{K_y} \sum_{n=1}^{K_x} \sum_{j=1}^{S} \chi^{(j)} V_{k,n}^{(j)} g[\mathbf{x} - \boldsymbol{\alpha}_{k,n} - \zeta(\lambda^{(j)})\mathbf{d}]. \qquad (4)$$

Note that function $J(\mathbf{x})$ of Eq. (4) may be expressed as a 2D spatial convolution $J = \Gamma \otimes g$ of the local macropixel intensity distribution $g(\Delta\mathbf{x})$ and of a "multichannel spectrometer" image $\Gamma(\mathbf{x})$ composed of nonoverlapping point sources $\delta[\mathbf{x} - \boldsymbol{\alpha}_{k,n} - \zeta(\lambda^{(j)})\mathbf{d}]$, with intensity $\chi^{(j)} V_{k,n}^{(j)}$ directly providing readings proportional to the spectral cube data $V_{k,n}^{(j)}$ in appropriately arranged spatial positions $[\boldsymbol{\alpha}_{k,n} + \zeta(\lambda^{(j)})\mathbf{d}]$. Whereas function $\Gamma(\mathbf{x})$ and spectral cube data $V_{k,n}^{(j)}$ are not directly available in an experiment, an approximating function $\hat{\Gamma}(\mathbf{x})$ may be restored from the single snapshot $J(\mathbf{x})$ by a "demultiplexing procedure" exploiting an appropriate deconvolution algorithm, under necessary restrictions on the signal-to-noise (SNR) ratio. This means that equipping a digital imaging system (camera) with a disperser and digital demultiplexing software indeed converts it into a snapshot SI system for macropixel images.

4. Row-wise Multiplexing and Demultiplexing Procedure

In a "row-wise" case in which the disperser's direction $\mathbf{d}$ of the chromatic dispersion coincides with axis x at the image sensor plane, macropixels extend only in a row direction, and there is no interaction between rows. Accordingly, for each row number $k = \overline{1, K_y}$ we can exploit one-dimensional (1D) notations by extracting a single row of the multiplexed spectrum 2D image. Figure 3 shows the formation of the row-wise multiplexed spectrum image with macropixels in a simplified case of only three spectral bands ($S = 3$) marked $\lambda_1, \lambda_2, \lambda_3$, where $S = 3$ is chosen in this figure only for graphical purposes and is not limiting.

The disperser shifts the light of each spectral band in every macropixel by one detector pixel relative to an adjacent spectral band, as described by the multiplexed spectrum image equation

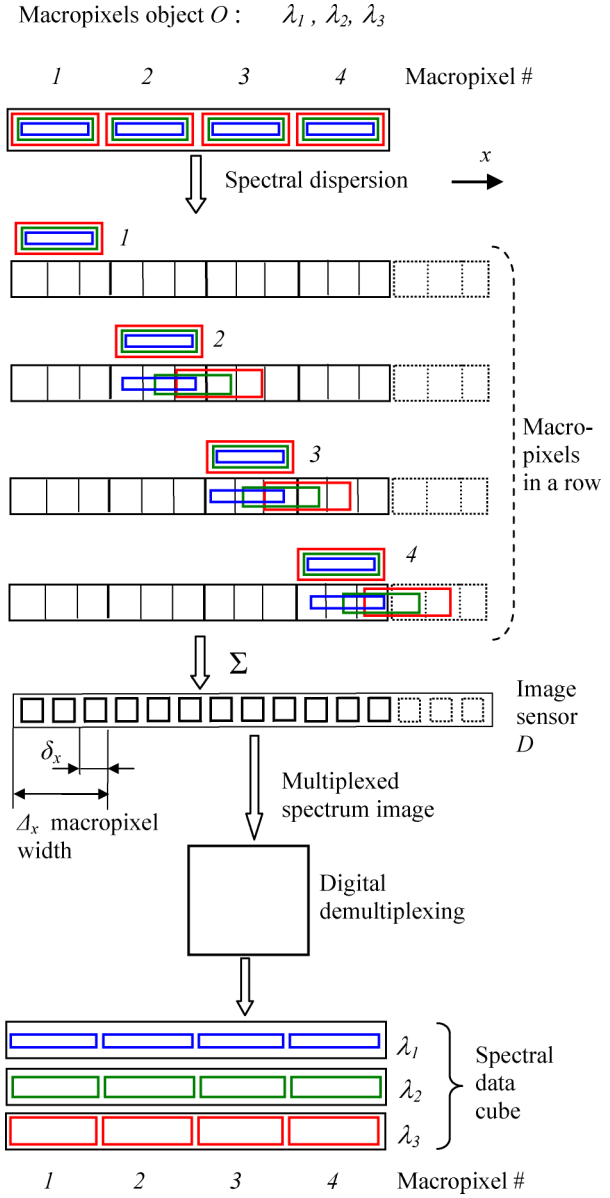

Fig. 3. (Color online) Formation of a row-wise multiplexed spectrum image with macropixels in a simplified case of only three spectral bands ($S = 3$) marked $\lambda_1, \lambda_2, \lambda_3$. The disperser (not shown) shifts the light of each spectral band in every macropixel by one detector pixel relative to an adjacent spectral band and induces overlaps. Digital processing demultiplexes the spectral data. δ_x is the image sensor pixel pitch, $\Delta_x$is the macropixel width.

$$J(x)=\sum_{n=1}^{K_x}\sum_{j=1}^{S}\chi^{(j)}V_{k,n}^{(j)}g\{x-[j_1+S_x(n-1)+j]\delta_x\},\tag{5}$$

which may be derived from Eq. (4) with

$$\alpha_n=[S_x(n-1)+1]\delta_x,\qquad \zeta(\lambda^{(j)})=[j_1+(j-1)]\delta_x,\tag{6}$$

where j_1 defines a dispersive image shift $j_1\delta_x$ at the first wavelength $\lambda^{(1)}$. The spectral shift described in Eq. (5) is similar to that considered in CTIS [9], but the local macropixel intensity distribution $g(\Delta x)$ is specific to our method.

The index $S_x(n-1)+j$ in Eq. (5) provides a linear ordering for successive spectra macropixels

$$\Gamma_{S_x(n-1)+j}=\chi^{(j)}V_{k,n}^{(j)},\qquad n=\overline{1,K_x},\qquad j=\overline{1,S},\qquad k=\overline{1,K_y},\tag{7}$$

such that each spectrum occupies the spatial extent of its macropixel. The entire dispersive shift of $\Delta\zeta=S\delta_x$ must not exceed the macropixel dimension $\Delta_x=S_x\delta_x$, to avoid macropixel spectra overlaps. An optimal match is $S=S_x$, which makes the number of image sensor pixels within a macropixel equal to the number of wavelength ranges that need to be resolved in SI, and which leads to $N_x=(K_x+1)S$. Equation (5) indicates that pixels J_m and $g_{\Delta m}$ of $J(x)$ and $g(\Delta x)$ are related by a discrete aperiodic 1D convolution

$$J_m=\sum_{\tilde{m}=1}^{K_xS_x}g_{m-\tilde{m}}\Gamma_{\tilde{m}},\qquad m=\overline{1,N_x},\qquad k=\overline{1,K_y},\tag{8}$$

with a narrow kernel $g_{\Delta m}$ extending by $S\ll N_x$ pixels.

The proposed digital demultiplexing procedure consists of two main stages, repeatedly applied to each row k of the multiplexed spectrum image $\{J_m\}$. First we restore $\{\hat{\Gamma}_m\}$ from $\{J_m\}$ of Eq. (8) using a 1D deconvolution algorithm accounting for the effects of noise, for example, the Lucy–Richardson algorithm [18,19]. Then, the spectral cube voxels $\{V_{k,n}^{(j)}\}$ are calculated by sorting and normalization as

$$V_{k,n}^{(j)}=\frac{\hat{\Gamma}_{S_x(n-1)+j}}{\chi^{(j)}},\qquad k=\overline{1,K_y},\qquad n=\overline{1,K_x},\qquad j=\overline{1,S}.\tag{9}$$

Note that each single value $V_{k,n}^{(j)}$ participates about S times in the S_x equations for the image sensor pixels. We consider this a main reason for the single snapshot image being sufficient for acquiring the entire spectral cube in our method, whereas other methods [6,12] require several images.

The proposed spectral multiplexing method of SI is restricted to macropixel objects such that macropixel sizes are properly matched to the dispersion and image magnification by a right design of the spectral imaging device, i.e., by adapting the prism, zoom of the camera, and distances for an application. There are important applications where a need for such adaptation is not restricting. For example, microarray plates used in enzyme-linked immunosorbent assay (ELISA) tests [15], DNA chips, and biochips with spotted microarrays [16,17] have only a few standard pitches but definitely provide a very wide class of macropixel objects in chemical and biological applications. Their optical reading can be easily adapted to snapshot spectral imaging as described here.

5. Experimental Results

Spectral imaging experiments were performed with macropixel objects created on a LCD monitor and composed of 24 × 19 small colored squares with spatially uniform intensities within each square. We targeted $S=32$ spectral bands for each macropixel.

The optical arrangement of the experiment, shown schematically in Fig. 2, included a commercial Canon EOS 30D digital camera equipped with a standard lens having a focal length of 18–55 mm and a standard 11°22′ wedge BK7 prism disperser positioned at a 1.9 m distance from the object. The prism dispersion in the visible spectrum range was chosen to match a macropixel width of $S_x=32$ image sensor pixels and to follow the direction of rows at the digital image. All experiments included spectral imaging of the objects, extraction of a 1D intensity array by vertical averaging of several strings within each of the 19 rows, digital data demultiplexing as described above, and subsequent comparison of the results with reference data. The latter was obtained from additional multiple-point slitlike objects that had thin colored vertical lines spaced at the same pitch as that of the macropixels so as to exclude any overlap of the spectrum from different slits. Therefore, the spectral imaging arrangement of Fig. 2, in a case of a slitlike object, served as a simple multichannel prism spectrometer, which provided direct measurements of a spectrum in a number of channels equal to the number of macropixels in the object.

The Canon EOS 30D digital cameras have good signal-to-noise characteristics and offer a monochrome black-and-white (B/W) mode that was used to collect the data in our experiments. As the camera pixels have red-green-blue (RGB) spectral filters and the algorithm of conversion from RGB to B/W is not known, we performed a direct measurement of the B/W mode image intensity depending on the object's intensity level. For that, we considered additional calibration patterns composed of 18 vertically arranged rectangles of about macropixel size having different levels of intensity, as seen on the left-hand side of

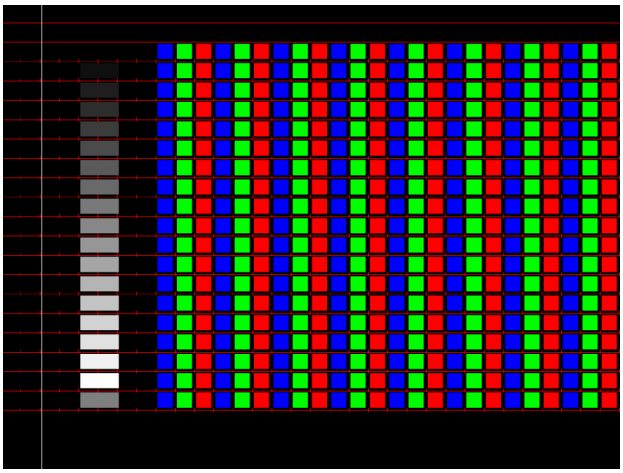

Fig. 4. (Color online) Macropixel object with periodically repeated RGB squares. Additional calibration patterns composed of 18 vertically arranged rectangles of about macropixel size having different levels of intensity are seen on the left side.

Fig. 4. The calibration patterns in each of the RGB colors were directly measured at the object plane by a silicon detector and correlated with appropriate B/W digital image data provided by the camera to find a nonlinearity curve for the intensity response. Subsequently, intensities of all the B/W mode camera images acquired in our experiments were compensated by an inverse nonlinearity, to provide light intensity pixels as an input for the demultiplexing algorithms.

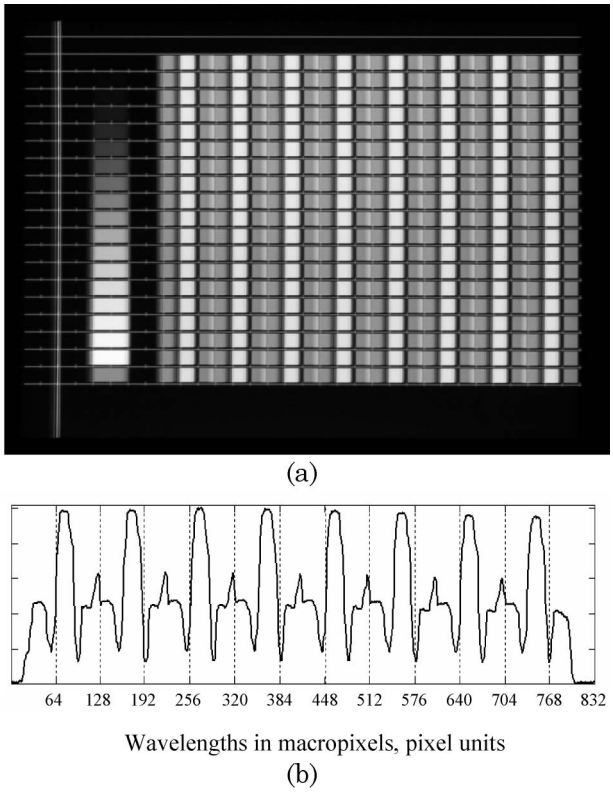

Fig. 5. Multiplexed sensor image of the RGB macropixel object: (a) monochrome B/W picture; (b) graph of a central row.

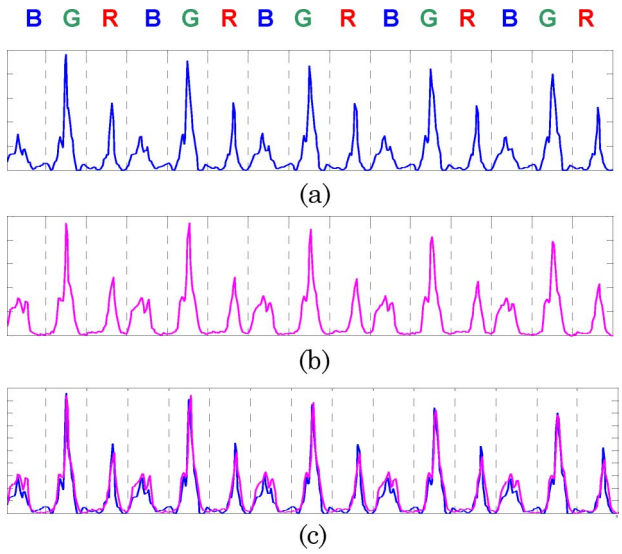

Fig. 6. (Color online) 32-band demultiplexed spectra of the central row of the RGB macropixel object, obtained by the digital deconvolution procedure of the multiplexed sensor image [blue curves at (a) and (c)] and, for comparison, a reference spectrum received from the slitlike RGB object [pink curves at (b) and (c)].

The first snapshot SI experiment was performed on a macropixel object with periodically repeated RGB squares (Fig. 4) and on a reference slitlike object in which the RGB squares were substituted by respective vertical RGB lines of the same color. The results are shown in Figs. 5 and 6. Figure 5(a) shows a B/W multiplexed sensor image of the RGB macropixel object of Fig. 4, having "spread" borders due to the chromatic dispersion and overlap of adjacent macropixels. Figure 5(b) shows a graph of a central row of Fig. 5(a). Figure 6(a) shows $S = 32$ band demultiplexed spectra of the RGB macropixel object obtained by the digital deconvolution procedure described above and applied to a central row of the multiplexed sensor image of Fig. 5(b). Figure 6(b) shows a graph of the directly measured dispersed image of

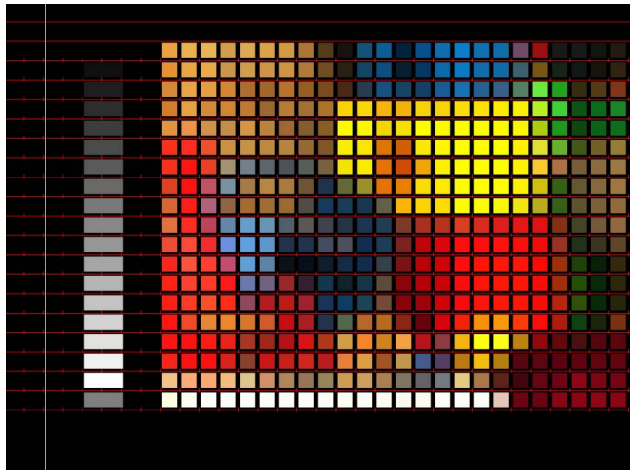

Fig. 7. (Color online) "Toys" macropixel object containing 24 × 19 square-shaped macropixels separated by a 15% black gap.

the reference slitlike RGB object, and Fig. 6(c) compares the graphs in Figs. 6(a) and 6(b). The comparison shows a good match in the spectral shape, peak positions, and height of the demultiplexed spectra of the macropixel object [Fig. 6(a)] with those of the directly measured slitlike reference spectra [Fig. 6(b)]. We conclude that our method works well for representation of RGB colors spectra with $S = 32$ spectral bands.

The second experiment was performed on multicolor 2D pictures using the same optical arrangement as in the first experiment. A "Toys" macropixel object in a low-resolution version containing 24×19 square-shaped macropixels separated by a 15% black gap, as shown in Fig. 7, was exhibited on the LCD monitor. Figure 8(a) shows its B/W multiplexed spectrum image, and Fig. 8(b) shows a graph of row 5 of the image. Figures 9(a) and 9(b) show, in a blue curve, $S = 32$ band demultiplexed spectra of the Toys object obtained by the digital deconvolution procedure applied on the graph in Fig. 8(b). This figure illustrates the exchange between spatial and spectral information, achieved by inserting a local spectrum with 32 spectral bands at every spatial position of a macropixel. Figure 9(c) shows a graph of the dispersed image of a reference slitlike Toys object, and Fig. 9(a) provides comparison of graphs Figs. 9(b) and 9(c). Finally, Fig. 10 shows the demultiplexed spectra and reference slitlike spectra for a few more sampled rows of the Toys macropixel object. A comparison of

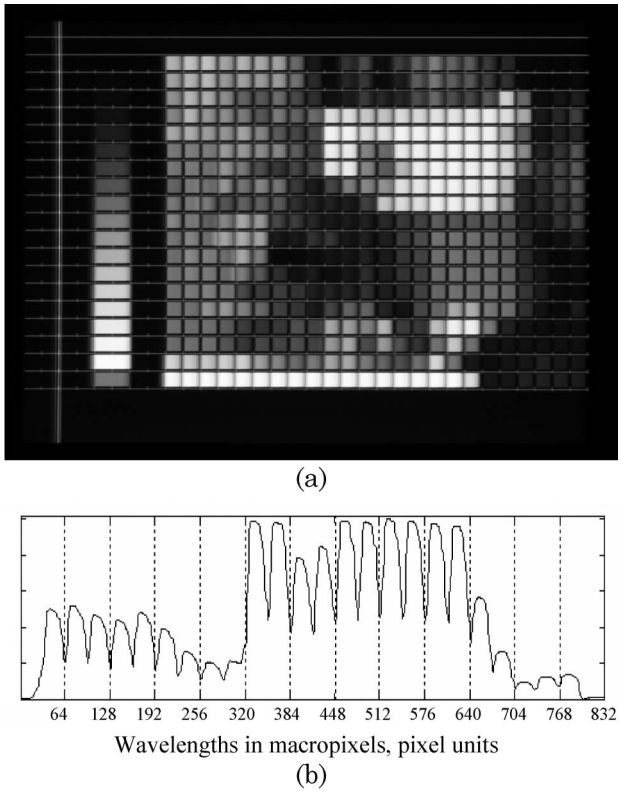

Fig. 8. Multiplexed spectrum image of the "Toys" macropixel object: (a) monochrome B/W picture; (b) graph of row 5.

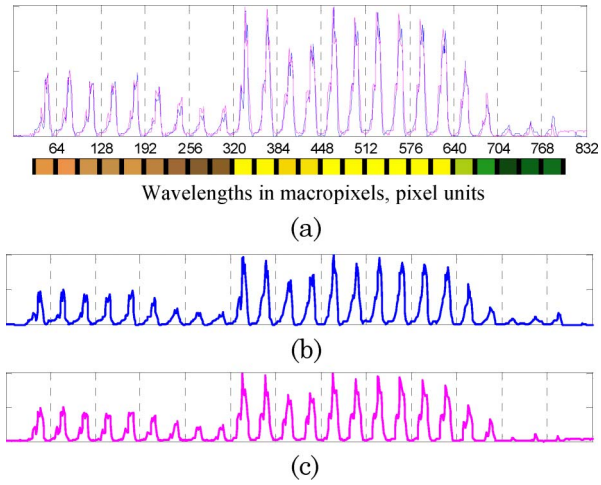

Fig. 9. (Color online) 32-band demultiplexed spectra of row 5 of the "Toys" macropixel object, obtained by the digital deconvolution procedure [blue curves in (a) and (b)] and, for comparison, a reference spectra of the reference slitlike "Toys" object [pink curves in (a) and (c)] . The color bar of respective macropixels is given only for illustration.

the spectral shape, peak positions, and height in the demultiplexed graph [blue curves in Figs. 9(a) and 10] with the directly measured reference spectrum [pink curves in Figs. 9(a) and 10] shows a good match between the demultiplexed Toys spectra and the reference spectra in respective 2D positions of the macropixel squares. Observed deviations from a perfect match may be explained by a residual nonlinearity of the camera response to the light intensity, by noise, and by the imperfectness of the laboratory level experimental setup, which may be further improved.

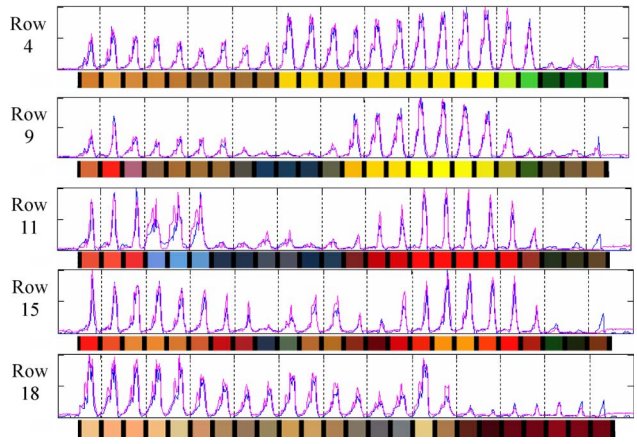

Fig. 10. (Color online) 32-band demultiplexed spectra of several rows of the "Toys" macropixel object, obtained by the digital deconvolution procedure (blue curve) and, for comparison, directly measured reference spectra of the slitlike "Toys" object (pink curve). Colors of respective macropixels are provided only for illustration. The graph shows both spectrum shape and intensity. The deviation of results is explained by nonlinearity, noise, and imperfectness of the lab level experimental setup.

6. Conclusions and Discussion

The spectrum multiplexing SI method proposed in this paper permits the conversion of a digital camera into a snapshot spectral imager by adding a disperser at the pupil of the imaging lens and by using appropriate data-demultiplexing algorithms. The method is applicable for objects that have a macropixel structure composed of small rectangles with an identical local spatial intensity distribution in every rectangle. The size of the macropixel is correlated with the compromise between the image spatial resolution and the number of spectral bands used in the spectral imaging. The lateral dispersive power of the disperser needs to match the macropixel size.

We would like to note that, in addition to multiplexing spectra on an image sensor and demultiplexing the result to recover a spectral image, our method has the following features that distinguish it from other SI methods.

a. The multiplexing is regular, with no aperture coding or randomization involved.

b. Our method does not require several projections of the spectral cube, field stop, or image relay, but directly exchanges spectral and spatial resolution.

c. The multiplexing corresponds to the macropixel structure of the image.

d. The multiplexing is done optically just by a disperser, and demultiplexing is done digitally.

e. The dispersion range needs to fit the size of the macropixel and image magnification.

f. The multiplexing and demultiplexing "pair" are carefully selected.

g. The resulting spectra are naturally arranged in a sequence matching exact positions of respective macropixels, so demultiplexing is contributed by optics, not only by digital processing.

h. The method works and provided 32 bands in a real experiment.

Our snapshot SI method is not limited to a particular region of the radiation spectrum but is applicable to any part of the spectrum that can be sensed with image sensor arrays, in particular the entire spectrum from the deep UV to the far IR. The absence of a slit provides increased light gathering efficiency, a very important advantage. Another important advantage is that the method does not require any moving or dynamic optical elements such as a rotating prism, filters scanning arrangements, or relay optics that inherently increase the size of an imager and restrict its speed. Consequently, SI systems based on this method are expected to be naturally amenable to miniaturization and low cost production for relevant applications.

The authors acknowledge Gershon Belitsky for support in carrying out the experiments.

References

1. Y. Garini, I. T. Young, and G. McNamara, "Spectral imaging: principles and applications," Cytometry A **69**, 735–747 (2006).
2. M. Brown, *Advanced Digital Photography* (Media Publishing, 2004).
3. R. L. Long, K. B. Walsh, and C. V. Greensill, "Sugar "imaging" of fruit using a low cost charge-coupled device camera," J. Near Infrared Spectrosc. **13**, 177–186 (2005).
4. M. A. López-Álvarez, J. Hernández-Andrés, and J. Romero, "Developing an optimum computer-designed multispectral system comprising a monochrome CCD camera and a liquid-crystal tunable filter," Appl. Opt. **47**, 4381–4390 (2008).
5. M. F. Carlsohn, "Spectral image processing in real-time," J. Real Time Image Process. **1**, 25–32 (2006).
6. M. Descour and E. L. Dereniak, "Computed-tomography imaging spectrometer: experimental calibration and reconstruction results," Appl. Opt. **34**, 4817–4826 (1995).
7. M. R. Descour, C. E. Volin, E. L. Dereniak, K. J. Thome, A. B. Schumacher, D. W. Wilson, and P. D. Maker, "Demonstration of a high-speed nonscanning imaging spectrometer," Opt. Lett. **22**, 1271–1273 (1997).
8. N. Hagen and E. L. Dereniak, "Analysis of computed tomographic imaging spectrometers. I. Spatial and spectral resolution," Appl. Opt. **47**, F85–F95 (2008).
9. W. R. Johnson, D. W. Wilson, and G. Bearman, "Spatial spectral modulating snapshot hyperspectral imager," Appl. Opt. **45**, 1898–1908 (2006).
10. J. Hartke and E. L. Dereniak, "Snapshot dual-band visible hyperspectral imaging spectrometer," Opt. Eng. **46**, 013201 (2007).
11. W. R. Johnson, D. W. Wilson, and W. Fink, "Snapshot hyperspectral imaging in ophthalmology," J. Biomed. Opt. **12**, 0140361 (2007).
12. J. M. Mooney, V. E. Vickers, M. An, and A. K. Brodzik, "High-throughput hyperspectral infrared camera," J. Opt. Soc. Am. A **14**, 2951–2961 (1997).
13. M. E. Gehm, R. John, R. Willett, T. Schultz, and D. Brady, "Single-shot compressive spectral imaging with a dual disperser architecture," Opt. Express **15**, 14013–14027 (2007).
14. A. Wagadarikar, R. John, R. Willett, and D. Brady, "Single disperser design for coded aperture snapshot spectral imaging," Appl. Opt. **47**, B44–B51 (2008).
15. D. Filippini, K. Tejle, and I. Lundstrom, "ELISA test for anti-neutrophil cytoplasm antibodies detection evaluated by a computer screen photo-assisted technique," Biosens. Bioelectron. **21**, 266–272 (2005).
16. H. Zhu, J. F. Klemic, S. Chang, P. Bertone, A. Casamayor, K. G. Klemic, D. Smith, M. Gerstein, M. A. Reed, and M. Snyder, "Analysis of yeast protein kinases using protein chips," Nat. Genet. **26**, 283–289 (2000).
17. P. O. Brown, "The full yeast genome on a chip," http://cmgm.stanford.edu/pbrown/yeastchip.html.
18. W. H. Richardson, "Bayesian-based iterative method of image restoration," J. Opt. Soc. Am. **62**, 55–59 (1972).
19. L. B. Lucy, "An iterative technique for the rectification of observed distributions," Astron. J. **79**, 745–754 (1974).